

Facile Fabrication and Integration of Patterned Nanostructured TiO₂ for Microsystems Applications**

By Abu Samah Zuruzi* and Noel C. MacDonald*

A simple technique to fabricate integrated crack-free and crystalline nanostructured titania (ns-titania) in microsystems devices is presented. In this technique, crack elimination is achieved by oxidizing Ti films, pre-patterned below a threshold dimension, in aqueous hydrogen peroxide solution. Amorphous ns-titania with walls of pores having thicknesses and pore diameters ranging from 25 nm–50 nm and 50 nm–200 nm, respectively, is formed after oxidation and transformed to anatase after thermal annealing. We demonstrate the functionality of ns-titania formed and compatibility of this technique with microsystems device manufacturing practices by fabricating a prototype device for gas sensing using integrated ns-titania features as sensing elements.

1. Introduction

The excellent properties of nanostructured titania (ns-titania) makes it the material of choice in many applications. Nanostructured titania has been reported to enhance the performance of implants^[1–3] and has recently been proposed as a vehicle for gene therapy.^[4] In addition to its biological uses, ns-titania finds applications in energy conversion,^[5] separation,^[6] catalysis,^[7] and gas sensing.^[8–10] A number of techniques have been developed for synthesizing porous titania, such as screen printing,^[5] reactive sputtering,^[8] anodizing,^[9] oxidation,^[10] emulsion templating,^[11] and sol-gel processing.^[12] Although the aforementioned techniques are satisfactory for some applications, use of high annealing temperatures (more than 600 °C) – which precludes use of standard aluminium-based metallization in microelectronic circuits – as well as issues of residual carbon incorporation, from organic precursors or binders, and crack formation in ns-titania layers, render these techniques unsuitable for microsystems device applications. Here we demonstrate a simple technique, which is compatible with microsystems device manufacturing, for integrating patterned ns-titania.

Aqueous oxidation of Ti surfaces is an attractive technique for growing ns-titania. Using aqueous hydrogen peroxide (aq. H₂O₂) solution as an oxidant, Wu et al.^[13] reported the formation of submicrometer-sized porous titania layers from thick sheets of Ti, while Tengvall and co-workers^[14–16] formed transparent bioactive titania gel from Ti powder and unpatterned films. Similarly, Nishiguchi et al.^[17] reported the formation of a porous titania layer by reacting Ti with aqueous NaOH solutions. However, the titania layers formed have high crack density, and delaminated extensively from the Ti substrate. In this paper, we report a technique that eliminates crack formation and delamination in titania layers by oxidizing Ti thin films that have been patterned below a threshold dimension. Also, the issue of carbon incorporation does not arise since no organic precursor is used. In addition, the patterning technique developed allows the fabrication of miniaturized ns-titania features and the formation of crystalline titania at relatively low temperatures, thus permitting the use of aluminium-based metallization. Hence, the technique described in this paper represents a practical route for fabricating and integrating ns-titania structures into Si-based microsystems devices.

2. Results and Discussion

We have investigated the formation of ns-titania on polished unpatterned bulk Ti sheets (500 μm thick) as well as unpatterned and patterned thin Ti films. Bulk Ti sheets were polished to a mirror finish before use. Ti thin films were electron-beam evaporated on 1 μm thick silicon dioxide (SiO₂) layer that had been thermally grown on Si pieces. Patterned Ti-pad arrays were fabricated using either lift-off or selective-masking techniques (see Figure 1). Exposure to aq. H₂O₂ results in the oxidation of Ti surfaces and the appearance of a dark-brown titanium oxide layer. Subsequently, the samples were blown dry in a gentle stream of nitrogen, dried further in air for 24 h, and annealed at 300 °C for 8 h. Various techniques were used to characterize the ns-titania layers formed.

[*] A. S. Zuruzi, Prof. N. C. MacDonald
Materials Department
and Mechanical and Environmental Engineering Department
University of California
Santa Barbara, CA 93106 (USA)
E-mail: nmacd@engineering.ucsb.edu

[**] The authors acknowledge stimulating discussions with Profs. A. G. Evans, M. Moskovits, C. R. Safinya, and Dr. Li Youli. Dr. A. Kolmakov and Dr. J. Lofvander are acknowledged for fruitful interactions. Partial support for this work was obtained from the Microsystems Technology Office of the Defence Advanced Research Projects Agency. This work made use of MRL Central Facilities supported by MRSEC Program of the NSF under Award No. DMR-00-80034. A. S. Z acknowledges the International Fellowship (National Science Scholars Program) from the Agency for Science, Technology and Research (Singapore).

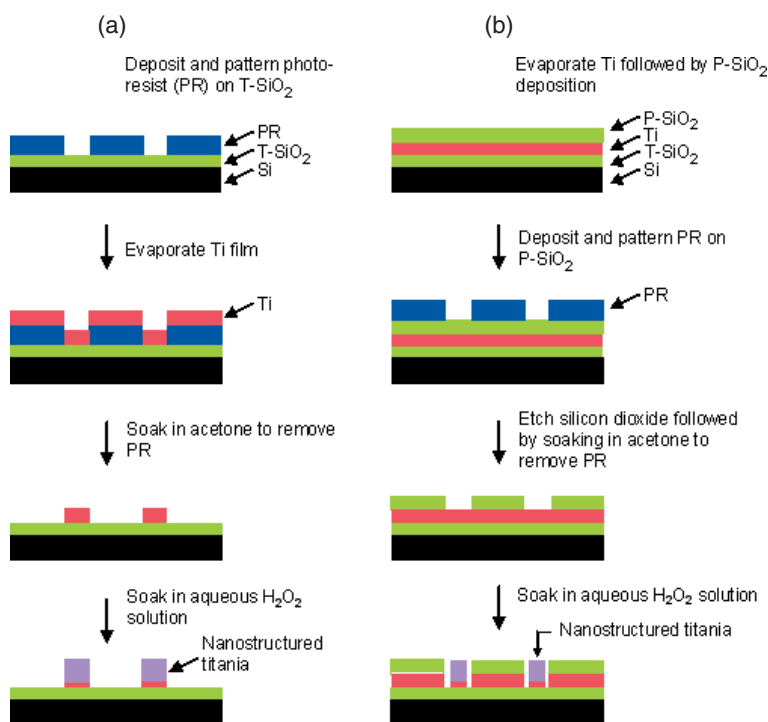


Figure 1. Schematic procedure to form ns-titania-pad arrays. a) The lift-off technique; b) the selective-masking technique.

Scanning electron microscopy (SEM) images of unpatterned bulk Ti sheets and Ti films after aging in aq. H₂O₂ revealed formation of ns-titania layers with high crack density (Figs. 2a–d). High-resolution SEM shows that the titania layers consist of walls of pores with thicknesses and pore diameters in the range 25 nm–50 nm and 50 nm–200 nm, respectively. The high crack

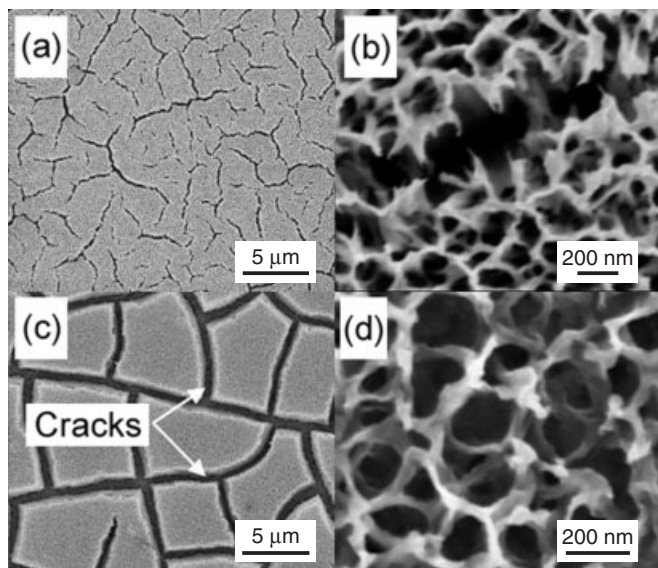


Figure 2. Crack formation in ns-titania layers formed on unpatterned Ti surfaces. SEM images of unpatterned a,b) bulk Ti sheets and c,d) Ti thin films showing high crack density in ns-titania formed on unpatterned Ti surfaces.

density results in the formation of ‘grains’ of about 5 μm–7.5 μm average diameter. Cracks on ns-titania layers formed on thin films extend from the surface to the thermally grown SiO₂ layer and resulted in complete delamination of ns-titania layers especially after prolonged oxidation times. The morphology of titania layers formed on bulk Ti sheets and evaporated Ti films is similar. However, delamination of ns-titania layers formed on bulk Ti sheets is less extensive and the cracks are narrower. In addition, pores in the ns-titania layer formed on bulk Ti sheets are smaller.

By using Ti films patterned below a threshold dimension, crack formation on ns-titania layers was eliminated. Figures 3a–e are SEM images of ns-titania layers formed from patterned Ti square pads of various dimensions after aging for 2.5 h at 80 °C in 10 vol.-% aq. H₂O₂ solution; the thickness of the Ti layer is 2.0 μm. Cracking is most extensive on the 100 μm pads and resulted in the ns-titania/unreacted Ti bilayer peeling off from the Si substrate (Fig. 3a, inset). Cracking is significantly reduced for the 70 μm pads, and for arrays of the 20 and 5 μm pads, crack formation is eliminated. In addition, gaps developed between the ns-titania/unreacted Ti bilayer and the mask

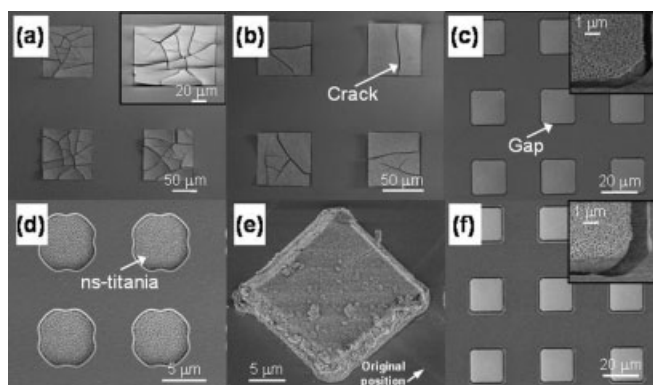


Figure 3. Crack elimination in ns-titania layers formed on Ti films patterned below a threshold dimension. SEM images of ns-titania layers formed on a) 100; b) 70; c,f) 20; and d) 5 μm pads using selective masking; and e) 20 μm pads using lift-off. Crack formation is eliminated for 20 and 5 μm pads. Comparison of a 20 μm pad array before (c) and after (f) annealing at 300 °C for 8 h shows an increase of gap width after annealing (see insets).

oxide. However, the ns-titania-pad arrays formed using the lift-off technique have little adhesion to the SiO₂ substrate and delaminate easily during aging in aq. H₂O₂ solution. Figure 3e shows a 20 μm ns-titania pad displaced from its original position. In contrast, ns-titania pads formed using selective masking have excellent adhesion to the underlying SiO₂ layer. Figure 3e also shows that ns-titania is formed on the sidewalls of pads formed using the lift-off technique. In contrast, ns-titania is not observed on the sidewalls of pads formed using selective

masking (Figs. 3c,e, inset). This observation suggests that gaps were formed during the latter stages or possibly after aging.

Cracks were not formed on 20 μm and 5 μm pads even after annealing at 300 °C for 8 h (Fig. 3f). However, the width of the gaps between the ns-titania/unreacted Ti bilayer and the mask oxide increased due to pad shrinkage. For 20 μm pads, the gap width was about 0.7 μm after drying in air, but increased to about 1.2 μm after annealing at 300 °C for 8 h (compare insets in Figs. 3c,f). For arrays of 5 μm pads, the width of the gap before and after annealing is estimated to be about 50 nm and 90 nm, respectively. These observations suggest that compressive forces are created in ns-titania layers during aging as well as during oxidation. This suggestion is further supported by the curvature (concave upwards) of the peeled-off titania/unreacted Ti bilayer (Fig. 3a, inset).

Cracks in ns-titania layers may start forming during oxidation, because of stresses due to thermal mismatch between ns-titania and residual titanium layers, and/or during drying, as a result of stresses associated with shrinkage. To elucidate the cause of crack formation, ns-titania arrays were observed while still in aq. H₂O₂ solution at room temperature, and again after drying. Figures 4a–c and Figures 4d–f are optical images of 20 μm, 40 μm, and 50 μm pad arrays of ns-titania before and after drying, respectively. In these experiments, 0.35 μm thick Ti films were completely oxidized to form supported TiO₂ membranes. Prior to drying, cracks were observed only on 50 μm ns-titania pads — it was found that 30 % of the pads were cracked (100 pads of each size were studied). After drying, cracks were observed on all pads of the 40 μm and 50 μm arrays — however, the 20 μm ns-titania-pad array remains crack-free. These observations indicate that crack formation in ns-titania is primarily due to stresses associated with shrinkage during drying. For ns-titania on 20 μm pads, this stress is not large enough to initiate cracks.

Focused-ion-beam milling was used to investigate the structural properties of ns-titania layers. Figures 5a,b are cross-sectional SEM images obtained after milling ns-titania layers grown on 2.0 μm thick evaporated Ti pads after aging in 10 vol.-%

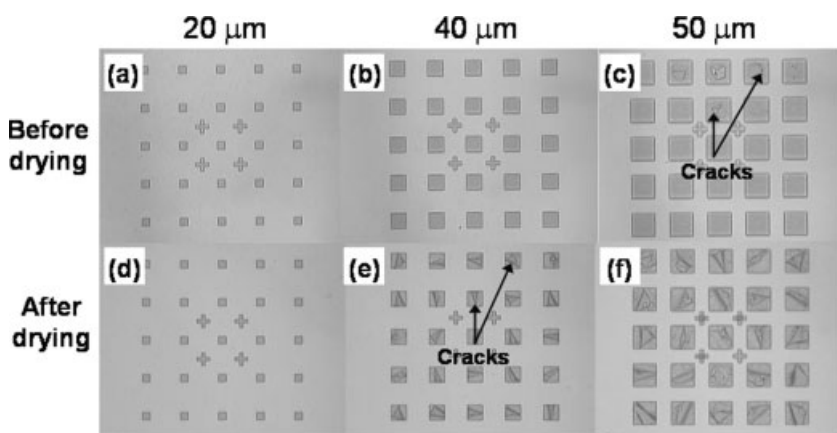


Figure 4. Crack formation in ns-titania-pad arrays during oxidation and drying steps. Optical microscope images of ns-titania arrays a–c) in aq. H₂O₂ after oxidation and d–f) after drying. These images clearly show that crack formation occurs primarily during the drying step. The pads in the arrays are 20, 40, and 50 μm squares as indicated.

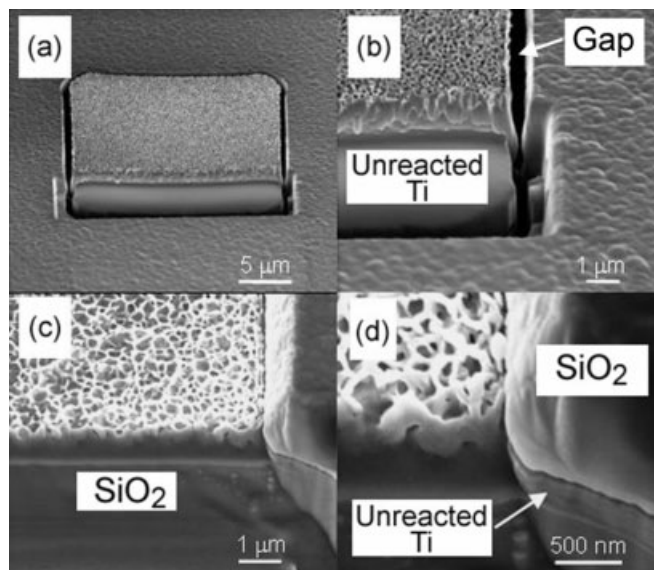


Figure 5. The structure of ns-titania layer interfaces. Cross-sectional SEM images obtained after milling. a,b) Nanostructured titania layers formed after partial oxidation of a 20 μm square-pad Ti film, 2.0 μm thick; c,d) ns-titania membranes formed after complete oxidation of a 0.35 μm thick Ti film.

aq. H₂O₂ for 2.5 h at 80 °C. The ns-titania/unreacted Ti interface is robust with no delamination. In addition, the ns-titania layers have uniform thickness with a planar ns-titania/unreacted Ti interface. Figures 5c,d are cross-sectional SEM images of supported TiO₂ membranes formed by oxidizing 0.35 μm thick evaporated Ti films by aging in 10 vol.-% aq. H₂O₂ for 3.5 h at 80 °C. Although the Ti films were completely oxidized, no cracks were observed on the 20 μm pad arrays. In addition, gaps between the ns-titania membranes and the mask oxide were not observed (Figs. 5c,d). This indicates that the thickness of the Ti films affects the extent of shrinkage of ns-titania patterns.

X-ray photoelectron spectroscopy (XPS) spectra of ns-titania layers suggest that aging in aq. H₂O₂ solution resulted in the formation of TiO₂ species only. Figures 6a,b are survey and high-resolution XPS spectra, respectively, of a ns-titania layer formed on an evaporated Ti thin film. Similar results were obtained for ns-titania layers formed on bulk Ti sheets. All spectra are referenced to the C1 s peak at 285.0 eV.^[18] Assuming a Tougaard background, the raw spectra were fitted using Gaussian–Lorentzian components with appropriate constraints for area, full width at half maximum, and position parameters using a commercial software (CasaXPS). From the analysis, binding energies for the Ti 2p_{3/2} components were found to be 459.0 eV and 458.9 eV for titania on bulk and evaporated Ti film, respectively. For ns-titania on bulk and evaporated thin-film Ti, the Ti 2p_{1/2} components have a value of 464.8 eV. These experimental values obtained are close to those

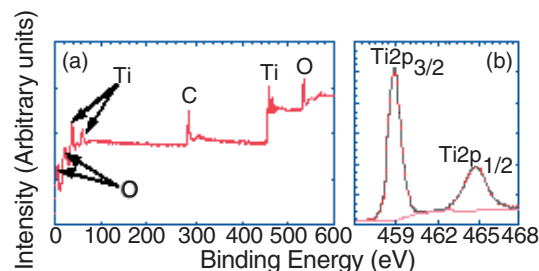


Figure 6. XPS spectra of TiO₂ species after drying. a) Survey and b) high-resolution XPS spectra of the ns-titania layer formed on an evaporated thin Ti film.

reported in the literature for TiO₂ of 458.9 eV and 464.6 eV for Ti 2p_{3/2} and Ti 2p_{1/2} components, respectively.^[19,20]

X-ray diffraction (XRD) studies show that amorphous TiO₂ and nanocrystals of anatase TiO₂ polymorph were formed after aging, and the amorphous phase transforms to anatase upon annealing. Figure 7a shows XRD spectra of an evaporated Ti film, as-aged, and an annealed TiO₂ layer formed from evaporated

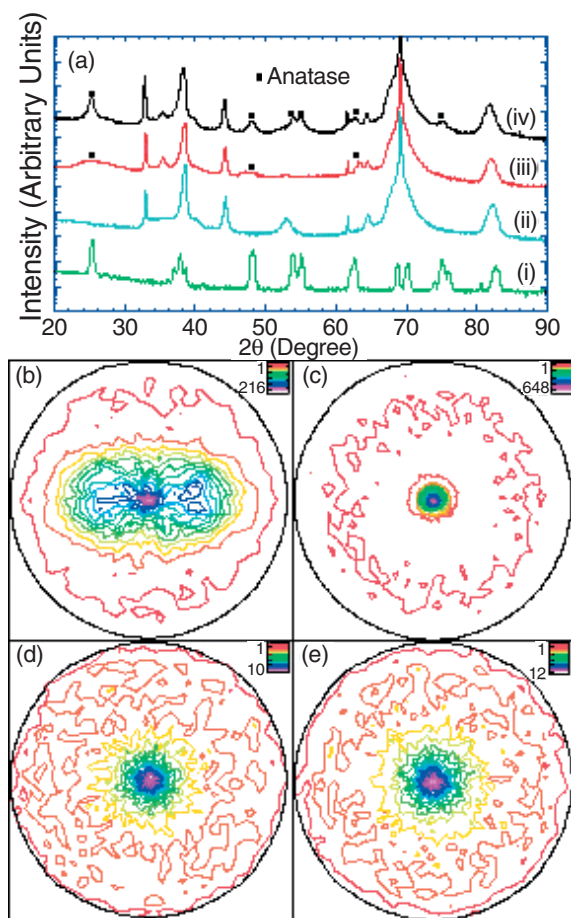


Figure 7. XRD spectra of TiO₂ species formed after aqueous oxidation. a) XRD spectra of i) the anatase reference sample, ii) the evaporated Ti film, and iii) the as-aged and iv) annealed ns-titania layer. The pole figures shown are for Ti {0002} of b) a Ti sheet and c) an evaporated thin Ti film, both before aging; and of anatase {101} collected after aqueous oxidation and annealing of d) bulk and e) thin-film Ti samples.

blanket Ti films. Spectra of the sample aged in 10 vol.-% aq. H₂O₂ solution for 2.5 h at 80 °C exhibit Ti peaks, which correspond to unreacted Ti in aged films, and three broad peaks at 2θ values of 25.20°, 47.97°, and 62.68°, which can be assigned to anatase {101}, {200}, and {204} planes. The broadness and low intensity of these peaks suggest that the as-formed titania layer consists of anatase nanocrystals in a largely amorphous titania matrix. Upon annealing at 300 °C for 8 h, these peaks sharpened significantly and increased in intensity. The peak sharpening and intensity increase upon annealing result from the transformation of the amorphous phase to anatase, which also agrees with the appearance of additional peaks at 2θ values of 53.91°, 54.95°, and 75.04°. These latter peaks correspond to the {105}, {211}, and {215} reflections of anatase. All anatase peaks in the spectrum of the annealed TiO₂ layer match perfectly to the corresponding ones in the spectrum collected from reference TiO₂ anatase powder (Alfa Aesar, 99.6 %). No peaks from other TiO₂ polymorphs are observed in spectra of annealed samples. Hence, XRD and XPS data indicate that only nanocrystals of anatase TiO₂ and an amorphous titania phase are formed after aging. Subsequent annealing transforms the amorphous phase to anatase. Formation of single-phase nanostructured anatase from amorphous TiO₂ by annealing in air, as well as the coexistence of these phases, had been reported previously.^[21,22]

X-ray pole-figure determination of bulk and thin-film Ti surfaces indicates that the orientation of anatase crystals formed during annealing is not influenced by the texture of the underlying Ti substrate – samples in this experiment are partially oxidized. Figures 7b,c are pole figures collected for Ti {0002} (2θ = 38.42°) of a bulk Ti sheet and an evaporated thin Ti film, respectively, before aging. These pole figures agree with other studies and are typical of hot-rolled Ti sheets and deposited thin Ti films, respectively.^[23,24] Figures 7d,e are the corresponding scans for anatase {101} (2θ = 25.20°), collected after aging in aq. H₂O₂ solution and subsequent annealing at 300 °C for 8 h. The similarity of Figure 7d and Figure 7e, and the narrow intensity range of these spectra, suggest that anatase crystals formed during annealing have a random orientation for both bulk and thin-film Ti, and that the texture of the underlying Ti substrate does not influence the orientation of these anatase crystals. This is in agreement with prior reports which showed that crystallization of anatase during annealing of amorphous TiO₂ layer takes place by the recrystallization of small anatase particles and the solid-state aggregation of amorphous particles.^[21] These mechanisms would be expected to produce randomly oriented anatase crystals.

Transmission electron microscopy (TEM) analysis of annealed samples confirms the formation of anatase after annealing. Figure 8a shows a cross-sectional image of a ns-titania pad formed after annealing. The ns-titania formed has a porous morphology with excellent adhesion to the thermally grown SiO₂ layer. Also, it was found that less than 5 % of titania remains as an amorphous phase after annealing, in agreement with a recent study.^[25] However, complete transformation could also be achieved with longer annealing times.^[21,25] Figure 8b shows the selected-area electron diffraction (SAED) pattern of region labeled A in Figure 8a which reveals the pres-

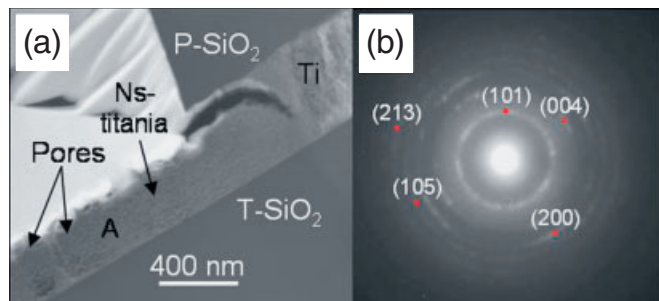


Figure 8. TEM analysis of annealed ns-titania. a) A TEM dark-field image and b) the SAED pattern of ns-titania of region labeled A in (a).

ence of only the anatase polymorph of titania. The ring diffraction pattern indicates that the titania formed is crystalline and that nanocrystals of anatase are randomly oriented in the walls of the pores. These observations are in agreement with XRD studies.

The porosity of the ns-titania layers obtained could be a result of the morphology of the intermediate gel layer formed during aging in aq. H₂O₂. The reaction of metallic Ti with hydrogen peroxide has been investigated by Tengvall and co-workers,^[14–16] and was shown to result in the formation of a hydrated TiO₂ gel layer. Recent studies by Wu et al. indicate that a submicrometer-sized porous layer resulted when this gel layer was annealed.^[13] However, no high-resolution microscopy images were given in these reports for comparison. It is suggested that the dark-brown layer that appears after aging in aq. H₂O₂ is a hydrated TiO₂ gel layer. The gel layers observed by Tengvall and co-workers were yellowish. However, the color difference could be attributed to the different concentration of aq. H₂O₂ solutions used.

Compared to other methods of forming ns-titania, the technique described in this article is compatible with current microsystems device manufacturing practices. As a demonstration of this compatibility, we have fabricated gas-sensor arrays with 20 μm ns-titania pads as sensing elements. Figure 9a is an optical microscopy image of a sensor array fabricated using a two-mask process — the inset is a single ns-titania pad with metallization. After annealing the ns-titania-pad array at 300 °C, the circuit was completed by deposition and development of a photoresist (PR) layer, followed by metal lift-off. The metallization consists of Ti/Pt layers of thickness 10 nm and 250 nm, respectively. Pt has been used to form contacts to TiO₂ (anatase),^[26] which is an n-type semiconductor. However, we found that Pt lines had poor adhesion to the SiO₂ mask layer and delaminated easily. A thin (10 nm) Ti layer evaporated before Pt prevents delamination of metallization lines on the SiO₂ mask. Figure 9b shows current–voltage (*I*–*V*) curves obtained from an integrated ns-titania pad at 250 °C under vacuum and at different oxygen partial pressures. The current measured decreased as oxygen partial pressure (and hence concentration) was increased, in agreement with other studies.^[26,27] The work function of semiconducting titania is sensitive to surface states created by gas adsorption, and this property has been utilized for gas-sensing applications.^[8–10,26] At 250 °C oxygen is

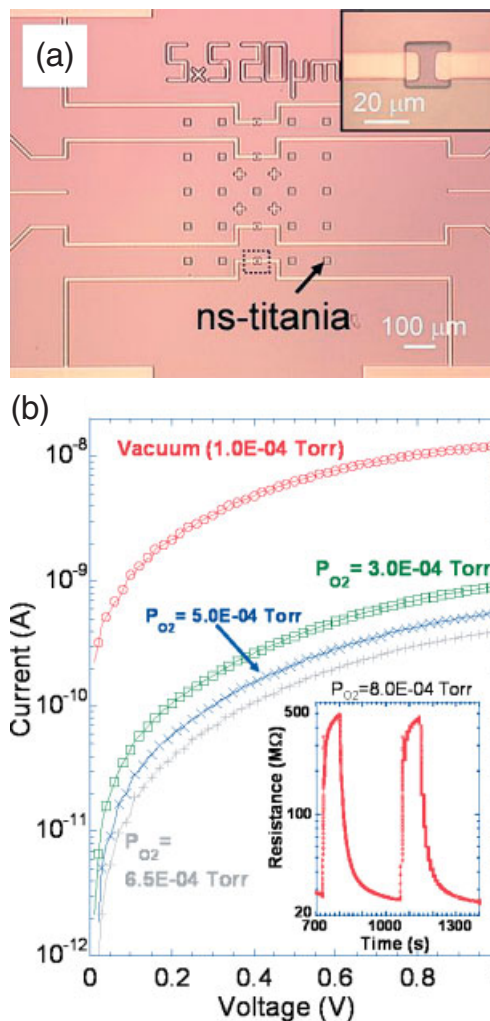


Figure 9. Integration of a ns-titania 20 μm pad array as resistive components in devices. a) A circuit with an integrated 5 × 5 array of ns-titania pads; inset: a magnified view of a single metallized ns-titania pad. b) *I*–*V* curve of a single ns-titania pad under various oxygen concentrations; inset: the resistance change when oxygen gas was introduced into the chamber at *t* = 725–800 s and at *t* = 1060–1145 s.

chemisorbed as singly charged anions which lead to electrons being trapped in surface states and a corresponding drop in conductance.^[26] With increasing oxygen concentration, this current reduction becomes more pronounced. The above results indicate that the surface properties of the integrated ns-titania pads are not affected by subsequent process steps necessary for integration, such as lithography, metal deposition, and lift-off.

The prototype gas-sensing device fabricated in this study exhibits superior sensitivity compared to other undoped-titania-based oxygen sensors reported in the literature. The sensitivity of a device is defined as the ratio of the maximum resistance in the presence of oxygen to resistance in the absence of oxygen (see Figure 9b, inset). The highest sensitivity to oxygen of the prototype device is 60, achieved at 200 °C with a corresponding response time of ~50 s. Response time is defined as the time needed for resistance to change from 10 % to 90 % of the maximum resistance when exposed to oxygen gas. Recently, Gao

et al., as well as Sharma and Bhatnagar, reported optimal sensitivity values of 1.43 and 30, respectively, for undoped-titania oxygen sensors at their operating temperature ranges.^[28,29] The latter study also reported an optimal response time of 8 s achieved at 600 °C, which is significantly less than that for the present study. Future research will focus on reducing the response time. Although long-term stability studies have not been carried out, no drift in device performance was observed after the device was held at 400 °C for a few hours; this was done repetitively over a few days. The gas-sensing stability of the fabricated device is attributed to the low residual amorphous titania that remained after annealing.

This study has demonstrated a technique for fabricating integrated ns-titania structures in microsystems devices. The technique utilizes process tools and materials commonly used in device manufacturing and offers the advantage of low annealing temperatures. Using this technique, ns-titania could be integrated in future Si-based microsystems devices to render functionalities of gas sensing, macromolecular separation, and catalysis, among others. In addition, by functionalizing the structures with appropriate chemical moieties, it may also be possible to use these fabricated ns-titania arrays as biomolecular sensors.^[30,31] Future research will explore use of ns-titania layers for these applications. We are also exploring the integration of ns-titania into Ti-based devices fabricated using bulk Ti micromachining technologies^[32] for biomedical applications, which leverage on the excellent biocompatibility of Ti.

3. Conclusions

A method of forming integrated and patterned nanostructured titania layers for microsystems applications has been demonstrated. Using Ti thin films patterned below a threshold area, crack formation on ns-titania layers can be eliminated. The ns-titania layers formed have a sponge-like morphology with pore diameters and wall thicknesses of about 50 nm–200 nm and 25 nm–50 nm, respectively. As-formed ns-titania is largely amorphous but transformed to anatase upon annealing at 300 °C. Crack formation in ns-titania layers occurs primarily during drying and is attributed to stresses associated with shrinkage. We have used this technique to integrate ns-titania pads as resistive components in circuits for gas sensing.

4. Experimental

We have investigated the formation of ns-titania on Ti bulk sheets and thin films. Bulk Ti sheets (Goodfellow, 99.6 % purity and 500 μm-thick) were first polished to a mirror finish with 0.3 μm colloidal silica and then rinsed copiously with de-ionized (DI) water (> 18.9 MΩ) with ultrasonic agitation. To prepare Ti thin-film samples, we used 2.5 cm × 2.5 cm pieces of n-type Si(100) (Mitsubishi Electronic Materials) as substrates. The Si pieces were first thermally oxidized at 1100 °C to grow a 1 μm thick SiO₂ layer. These were then cleaned with ultrasonic agitation for 5 min each in acetone, 2-propanol, and de-ionized (DI) water (18.9 MΩ), and blown dry with nitrogen prior to deposition of Ti films. A schematic flow diagram for formation of ns-titania on patterned Ti-pad arrays is shown in Figure 1. Ti thin films were pat-

terned using either lift-off or selective-masking process. In selective masking, the Ti film was electron-beam evaporated on Si pieces followed by silicon dioxide deposition. Silicon dioxide was deposited using plasma-enhanced chemical vapor deposition using silane (SiH₄) and nitrous oxide (N₂O) precursors at 250 °C. Photoresists (PRs) were deposited on the silicon dioxide layer and patterned. The pattern on the PR layer was transferred to the silicon dioxide layer by etching with CHF₃ gas. After patterning, the PR was removed by soaking in acetone. In the lift-off technique, a PR layer was deposited on Si pieces and patterned. Ti film was then evaporated. The Si pieces were then soaked in acetone for 24 h, rinsed sequentially in 2-propanol and DI water, and blown dry. For depositing blanket Ti films, the Si pieces were used as cleaned. The process pressure during evaporation of Ti films was ~5.0 × 10⁻⁷ torr. All Ti sources used were of 99.995 % purity or better, and cleaned by pre-evaporation to remove the native oxide layer from the surface.

Nanostructured titania was formed by aging samples in aqueous H₂O₂ solution. Prior to aging, Ti films were acid pickled in dilute HCl acid for ~2 min to remove the native oxide layer, rinsed in DI water, and then blown dry with nitrogen. Aging was done in an oven at 80 ± 2 °C in air. Samples were stored in a vacuum box prior to analysis. Crystal structure was analyzed by X-ray diffraction in Bragg-Brentano configuration using Cu Kα radiation (1.5406 Å) (Phillips X'pert-MPD). Structural characterization was done using an FEI dual-beam focused-ion-beam system equipped with Ga-ion and electron columns for high-resolution machining and imaging operations, respectively. Micromachining was done using a Ga-ion current of 100 pA. Surface chemical species were determined using a Kratos Axis Ultra X-ray Photoelectron Spectroscopy (XPS) system. High-resolution XPS scans were obtained with a monochromated Al Kα source (1486.6 eV) and 20 eV pass energy, with steps of 0.05 eV at a base pressure of 7.5 × 10⁻⁹ torr. The XPS spectra collected were fitted to line shapes constructed from a linear combination of Gaussian and Lorentzian profiles using commercial software (CasaXPS N. Farley, version 2.2.0 Dev 16, 1999) Transmission electron microscopy was carried out using an FEI Sphera T20 machine operating at 200 kV. Performance of the prototype gas sensor was evaluated using a test station where an appropriate amount of oxygen was introduced into a chamber using mass-flow controllers and the electrical response of the sensor was monitored.

Received: March 30, 2004

Final version: August 12, 2004

- [1] F. Heidenau, F. Stenzel, G. Ziegler, *Key Eng. Mater.* **2000**, 192–I, 87.
- [2] D. M. Brunette, P. Tengvall, M. Textor, P. Thomsen, *Titanium in Medicine: Materials Science, Surface Science, Engineering, Biological Responses and Medical Applications*, Springer-Verlag, New York **2001**.
- [3] T. J. Webster, R. W. Siegel, R. Bizios, *Biomaterials* **1999**, 20, 1221.
- [4] T. Paunesku, T. Rajh, G. Wiederrecht, J. Maser, S. Vogt, N. Stojicevic, M. Protic, B. Lai, J. Oryhon, M. Thurnauer, G. Woloschak, *Nat. Mater.* **2003**, 2, 343.
- [5] M. Grätzel, *Nature* **2001**, 414, 338.
- [6] J. Kim, K. C. Song, O. Wilhelm, S. E. Pratsinis, *Chem. Ing. Tech.* **2001**, 73, 61.
- [7] M. P. Harold, C. Lee, A. J. Burggraaf, K. Keizer, V. T. Zaspalis, R. S. A. Delange, *MRS Bull.* **1994**, 19, 34.
- [8] G. Sberveglieri, L. E. Depero, M. Ferroni, V. Guidi, G. Martinelli, P. Nelli, C. Perego, L. Sangaletti, *Adv. Mater.* **1996**, 8, 334.
- [9] O. K. Varghese, D. W. Gong, M. Paulose, K. G. Ong, E. C. Dickey, C. A. Grimes, *Adv. Mater.* **2003**, 15, 624.
- [10] P. I. Gouma, M. J. Mills, K. H. Sandhage, *J. Am. Ceram. Soc.* **2000**, 83, 1007.
- [11] A. Imhof, D. J. Pine, *Nature* **1997**, 389, 948.
- [12] K. Kajihara, K. Nakanishi, K. Tanaka, K. Hirao, N. Soga, *J. Am. Ceram. Soc.* **1998**, 81, 2670.
- [13] J. M. Wu, S. Hayakawa, K. Tsuru, A. Osaka, *Scr. Mater.* **2002**, 46, 101.

- [14] P. Tengvall, *Ph.D. Thesis*, Linköping University, Sweden **1989**.
- [15] P. Tengvall, I. Lundstrom, L. Sjoqvist, H. Elwing, L. M. Bjurstein, *Biomaterials* **1989**, *10*, 166.
- [16] P. Tengvall, H. Elwing, I. Lundstrom, *J. Colloid Interface Sci.* **1989**, *130*, 405.
- [17] S. Nishiguchi, S. Fujibayashi, H. M. Kim, T. Kokubo, T. Nakamura, *J. Biomed. Mater. Res.* **2003**, *67A*, 26.
- [18] J. F. Moulder, W. F. Stickle, P. E. Sobol, K. D. Bomben, *Handbook of X Ray Photoelectron Spectroscopy: A Reference Book of Standard Spectra for Identification and Interpretation of XPS Data*, Physical Electronics Inc., Eden Praire, MI **1995**.
- [19] T. Choudhury, S. O. Saied, J. L. Sullivan, A. M. Abbott, *J. Phys. D.* **1989**, *22*, 1185.
- [20] D. Gonbeau, C. Guimon, G. Pfisterguillouzo, A. Levasseur, G. Meunier, R. Dormoy, *Surf. Sci.* **1991**, *254*, 81.
- [21] H. Z. Zhang, M. Finnegan, J. F. Banfield, *Nano Lett.* **2001**, *1*, 81.
- [22] S. Z. Chu, K. Wada, S. Inoue, S. Todoroki, *Chem. Mater.* **2002**, *14*, 266.
- [23] J. P. Gueneau de Mussy, G. Langelaan, J. Decerf, J.-L. Delplancke, *Scr. Mater.* **2003**, *48*, 23.
- [24] B. Major, R. Ebner, P. Zieba, W. Wolczynski, *Appl. Phys. A* **1999**, *69*, S921.
- [25] A. Ruiz, A. Calleja, F. Espiell, A. Cornet, J. R. Morante, *IEEE Sens. J.* **2003**, *3*, 189.
- [26] K. D. Schierbaum, U. K. Kirner, J. F. Geiger, W. Göpel, *Sens. Actuators B* **1991**, *4*, 87.
- [27] N. Savage, B. Chwieroth, A. Ginwalla, B. R. Patton, S. A. Akbar, P. K. Dutta, *Sens. Actuators B* **2001**, *79*, 17.
- [28] L. Gao, Q. Li, Z. Song, J. Wang, *Sens. Actuators B* **2000**, *71*, 179.
- [29] R. K. Sharma, M. C. Bhatnagar, *Sens. Actuators B* **1999**, *56*, 215.
- [30] J. H. Yu, H. X. Ju, *Anal. Chem.* **2002**, *74*, 3579.
- [31] H. H. Yu, S. Q. Liu, H. X. Ju, *Biosens. Bioelectron.* **2003**, *19*, 509.
- [32] M. F. Aimi, M. P. Rao, N. C. MacDonald, A. S. Zuruzi, D. P. Bothman, *Nat. Mater.* **2004**, *3*, 103.